Marshall Plan Scholarship 2011

Final Report

High Power Impulse Magnetron Sputtering (HiPIMS) of Niobium Thin Films

Submitted by

Albert Rauch

to the

Austrian Marshall Plan Foundation

Ungargasse 37, 1030 Vienna, Austria

Scholarship holder: Albert Rauch
Torkelweg 7
6824 Schlins, Austria
Phone: +43 650 9753106
Email: albertrauch@gmx.at

Period of time: 11th January 2011 to the 26th October 2011

Field of study: Thin film technology

Research topic: High Power Impulse Magnetron Sputtering (HiPIMS) of Niobium Thin Films
Plasma potential measurements with pulsed emissive probes

Home institution: Institute for Thin Film Technology
Leopold-Franzens-University Innsbruck
Technikerstrasse 25
A-6020 Innsbruck, Austria
Web: http://www.uibk.ac.at/ionen-angewandte-physik/tft/

Advisor at home institution: Prof. Dr. Hans K. Pulker
Tel.: +43 (0)512 507-6248
Fax: +43 (0)512 507-2932
e-mail: hans.pulker@uibk.ac.at

Advisor at host institution: Dr. André Anders, Senior Physicist
Leader, Plasma Applications Group
Lawrence Berkeley National Laboratory
One Cyclotron Road, MS 53
Berkeley, CA 94720, USA
Ph: (510) 486-6745
Fax: (510) 486-4374
e-mail: aanders@lbl.gov

Abstract:

High Power impulse magnetron sputtering (HIPIMS) is a relatively young physical vapor deposition (PVD) technology that combines magnetron sputtering with pulsed power technology, where the peak power exceeds the time-averaged power by typically two orders of magnitude. The peak power density, averaged over the target area, can reach or exceed 10^7 W/m^2, leading to plasma conditions that make ionization of the sputtered atoms very likely. The objective is to achieve ionization of the sputtered atoms in order to have ions available for substrate etching (pre-treatment) and/or for assistance to the film growth process, leading to a well adherent coating of desirable microstructures and properties.

Niobium (Nb) coatings on copper cavities have widely been seen as a cost-efficient replacement of bulk niobium cavities, however, coatings made by magnetron sputtering have not lived up to high expectations.

The development of deposition of thin Niobium (Nb) films onto Copper (Cu) cavities shows a clear advantage compared to bulk niobium, in particular for low frequencies or for operations at 4.2 K.

- Better thermal stability (resistance to "'quench"') thanks to the much higher thermal conductivity of the OFE copper substrate compared to the superconducting niobium
- Reduced material cost
- Possibility of applying high *Tc* coatings (*NbTiN, V_3Si,Nb_3Sn*)

The first sputtering techniques were performed at CERN in the early 1980´s. The sputter coating technology was chosen as a basis for development in a magnetron setup. During the last decades a lot of effort was put in to understand the possibilities and disadvantages of this technique. As one of the newest developments in coating technology High-Power Impulse Magnetron Sputtering (HiPIMS) was introduced in the late 1990´s as a physical vapor deposition. At an early stage in their use however, it was recognized that through plasma diagnostic techniques, such as electrostatic probing and emission spectroscopy, information on particle concentrations and temperatures could lead to a better understanding of these complex magnetized discharges and aid in their better understanding.
One area which has received little attention, however, is the structure of the plasma potential V_P in front of the target. In this work, we apply a new method to examine in detail the distribution of V_P in

a HiPIMS discharge and gain new information on the electric field. Knowledge of V_P is generally important in plasma discharges because it reveals the electric field structure in the plasma volume, it defines the potential at which ions are generated and hence determines their bombarding energies at the substrate and it affects charge particle transport and the overall distribution of electron and ion plasma densities in the discharge.

REVIEW OF SCIENTIFIC INSTRUMENTS 82, 093505 (2011)

A synchronized emissive probe for time-resolved plasma potential measurements of pulsed discharges

Jason M. Sanders,[1,2] Albert Rauch,[1] Rueben J. Mendelsberg,[1] and André Anders[1,]

[1]*Lawrence Berkeley National Laboratory, University of California, Berkeley, California 94720, USA*

[2]*Department of Electrical Engineering, University of Southern California, Los Angeles, California 90089, USA*

(Received 5 July 2011; accepted 29 August 2011; published online 27 September 2011)

A pulsed emissive probe technique is presented for measuring the plasma potential of pulsed plasma discharges. The technique provides time-resolved data and features minimal disturbance of the plasma
achieved by alternating probe heating with the generation of plasma. Time resolution of about 20 ns is demonstrated for high power impulse magnetron sputtering (HIPIMS) plasma of niobium in argon. Spatial resolution of about 1 mm is achieved by using a miniature tungsten filament mounted on a precision translational stage. Repeated measurements for the same discharge conditions show that the
standard deviation of the measurements is about 1-2 V, corresponding to 4%-8% of the maximum plasma potential relative to ground. The principle is demonstrated for measurements at a distance of 30 mm from the target, for different radial positions, at an argon pressure of 0.3 Pa, a cathode voltage
of -420 V, and a discharge current of about 60 A in the steady-state phase of the HIPIMS pulse.

I. INTRODUCTION

Emissive probes have been used in a variety of plasma environments to determine important plasma properties, including the plasma potential, ion density, electron density, and electron temperature.[1–3] First described by Langmuir in 1923, electron emitting probes consist of a thin metal wire filament, typically made from tungsten, that is heated to high temperature with a current in order to achieve thermionic emission.[4] When immersed in plasma, a sheath forms around the surface of the filament. The sheath thickness is governed by a number of factors, including the difference between plasma

potential and probe potential, and the temperature of the probe's filament, which determines thermionic electron emission. Measuring the balance of electron current emitted from the probe and the particle currents to the probe provides an accurate method for determining the local potential of the plasma. Emissive probes are often preferable to collecting probes for determining the plasma potential because emissive probes are capable of providing the measurement directly. To show the advantages, we first consider the theory of cold, non-emitting probes. The plasma potential Φ can be calculated via

$$\Phi = V_f + \frac{k_B T_e}{q} \ln\left(\frac{I_{es}}{I_{is}}\right), \quad (1)$$

where V_f is the floating potential, T_e is the electron temperature, I_{es} is the electron saturation current, I_{is} is the ion saturation current, k_B is the Boltzmann constant, and q is the average charge of the ions. This indirect measurement technique requires knowledge of the electron temperature, which can fluctuate during the measurement, and mean ion charge state, which is often but not always close to unity. Furthermore, *Eq. (1)* is valid for electron velocity distributions that are Maxwellian; so, the calculated plasma potential will be erroneous for the highly magnetized, pulsed plasmas used in some processing techniques.

Emissive probes remove much of this uncertainty because the current measured as a function of probe bias for the emitting probe diverges from that measured for a collecting probe only when the bias voltage is less than the plasma potential. Therefore, the plasma potential can be determined by comparing an emissive probe's *I-V* curve to a collecting probe's *I-V* curve.[5] Furthermore, as the emission of the probe increases, the probe's floating potential shifts toward the plasma potential enabling time-resolved measurements of the probe potential by measuring the probe's floating voltage.[6]

This shift in the floating potential can be understood by considering a modified version of Eq. (1) that accounts for the current emitted from the probe,[7]

$$\Phi = V_f + \frac{k_B T_e}{q} \ln\left(\frac{I_{es}}{I_{is} + I_{em}}\right), \quad (2)$$

where I_{em} denotes the electron current emitted from the probe.

The emission currents need to be added to the ion saturation current because a current of (negative) electrons emitted from the probe is electrically equivalent to a current of (positive) ions collected by the probe. Equation (2) shows that the floating potential V_f of the probe approaches the plasma potential as the emitted current from the probe increases. V_f attains the plasma potential Φ for $I_{em} = I_{es} - I_{is}$. Further increase of I_{em} will not lead to a further growth of the potential of the probe, because

it is saturating. A more detailed theoretical treatment of how the floating potential behaves in the presence of electron

emission can be found in previously published papers.[8]

In addition to these two methods of measuring the plasma potential, typically referred to as the divergence point method and the saturated probe method, respectively, there is the inflection point method where the plasma potential is readily identified by the inflection point of the characteristic via

its first derivative.[5, 9, 10] This method, however, is less suitable for transient or noisy plasmas. For these plasmas, the saturated probe method is the most straightforward way to evaluate the plasma potential. The accuracy of the measurement is typically about 1 V for well-controlled operating conditions.[10] The saturated probe method has been used successfully to make measurements in non-Maxwellian, magnetized plasmas,[2, 7, 11] even as this method is susceptible to perturbations by magnetic fields, which must be taken into account. In Sec. II, we will apply the saturated probe method and show the feasibility of pulsed heating to minimize plasma disturbance and enhance accuracy of measurements.

II. PULSED PROBE PRINCIPLE AND DESIGN

The basic principle of an emissive probe requires altering the characteristics of a single probe through thermionic emission of electrons by ohmic heating of the probe using a heating current (Fig. 1). When the probe potential is more positive than V_P, the probe current is unchanged by the emission of the thermal electrons, because the emitted electrons cannot escape the probe's sheath and are repelled by the plasma and return to the probe. The temperature of the emitted electrons is equal to the wire temperature, corresponding to about 0.2 eV, which is much less than the energy of the plasma electrons. When the applied probe bias becomes negative relative to V_P, the emitted thermal electrons are accelerated away from the probe, and thus, the measured probe current becomes increasingly greater until it saturates, indicating that all of the emitted electrons and arriving ions are measured, while all of the plasma electrons are repelled.

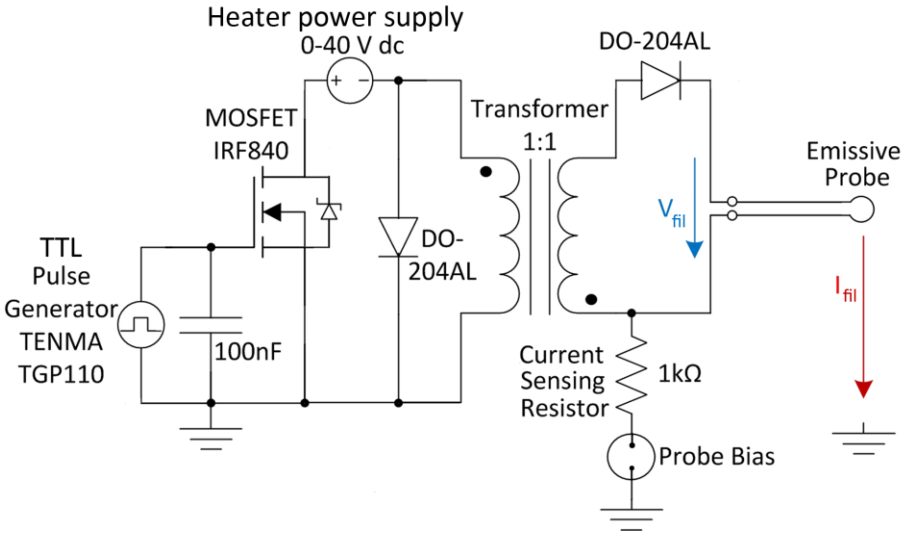

FIG. 1. (Color online) A simplified schematic of the circuit used to pulse the probe´s tungsten filament. A capacitor at the gate of the power MOSFET slows the turn-on time and reduces transients from switching the floating power supply.

In this work, a synchronized, pulsed emissive probe measurement station has been designed to measure the potential of pulsed plasmas. In the design used here, the glowing probe tip was made from a tungsten coil taken from a Mini Mag Lite 2-cell AA flashlight xenon replacement bulb. A diamond saw was used to carefully cut the glass casing, which provided us with the 1 mm long solenoid made from a 30 µm tungsten wire conveniently attached to the socket with its two contact pins (Fig. 2).

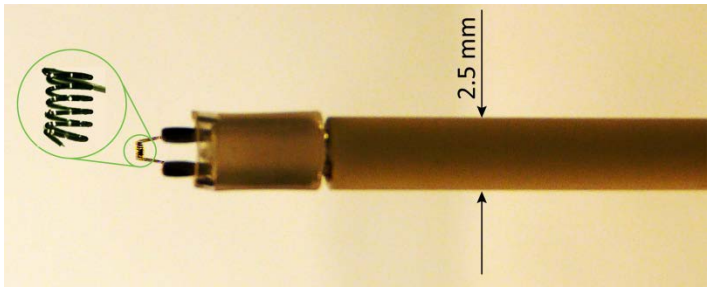

FIG. 2. (Color online) An image of the probe; the tungsten filament has a 30 µm diameter wire, a coil diameter of 240 µm, a coil length of about 1 mm, and a total wire length of about 6 mm.

The miniature solenoid consists of six turns, each turn having a diameter of approximately 240 µm. The bulb was push fit into a 2.5 mm diameter, 150 mm long ceramic stem and aligned in radial direction in the plasma volume (Fig. 3). Electrical connection to the probe was made via a twisted pair fed through the ceramic tube. Of course, this specific design is not critical for the operation of a pulsed, synchronized emissive probe. For other measurements, to be reported elsewhere, a simple loop of fine tungsten wire was used.

Typically, the probe's heating current is provided by an ac current source that is electrically isolated from ground via a transformer.[6, 11–13] By heating the filament with a pulse before the plasma pulse is generated and switching heating off when the plasma is on, as illustrated in Fig. 4, the electric field established by the forward voltage drop across the tungsten filament will not exist when the plasma is present. Pulsing the heating current allows us to use a tungsten coil filament from a miniature light bulb since without pulsing; the heating current flowing through the coil would produce a non-negligible magnetic field. This issue is avoided by the timing of heating. Calculations showed that the magnetic field of the light bulb solenoid generated by the heating current is about 16%-23% of the local magnetic field of the magnetron's permanent magnets, at the locations of measurement. The ability to use filaments from a readily available commercial bulb reduces the cost of the probe and allows for simple replacement should the filament be damaged.

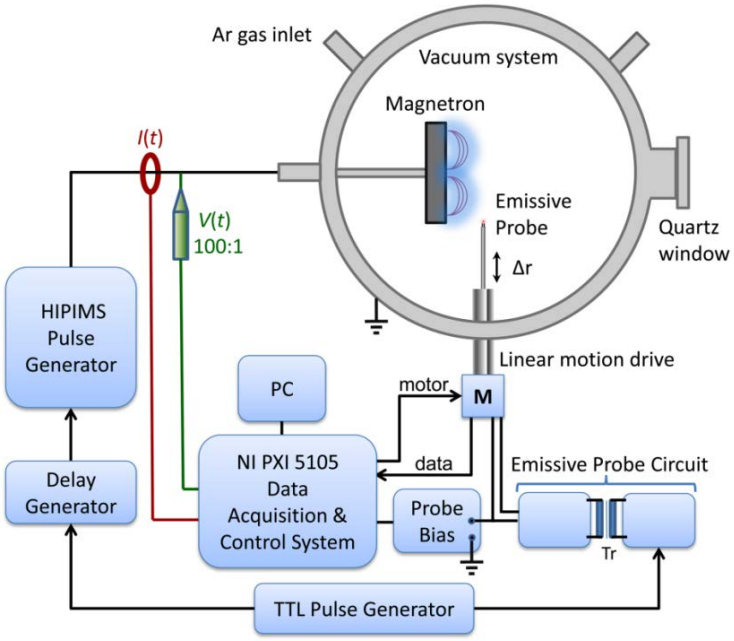

FIG. 3. (Color online) The emissive probe tested in a HIPIMS experiment vacuum chamber. The probe´s position is automatically controlled relative to the symmetry axis of the magnetron in 30 mm distance from the surface of the target. Plasma is generated by a planar magnetron that is driven by a HIPIMS pulse generator.

This pulsed emissive probe system readily integrates with common pulsed plasma processing techniques because typical plasma duty cycles are less than 20%, which leaves enough time to heat the probe's filament into strong thermionic emission during the plasma's off-time.[14] We show that the droop in thermionic emission during the discharge can be kept small, which means the emission is nearly constant, as if the probe is heated continuously. The filament can be sufficiently heated to achieve strong enough emission such that measurements can be made using the *saturated probe method* mentioned above. As an example of a practical implementation of the principle, measurements of the plasma potential will be presented for a 7.6 cm diameter Nb target that is

pulsed in the high power impulse magnetron sputtering (HIPIMS) mode in argon at 0.33 Pa and 0.28 Pa.

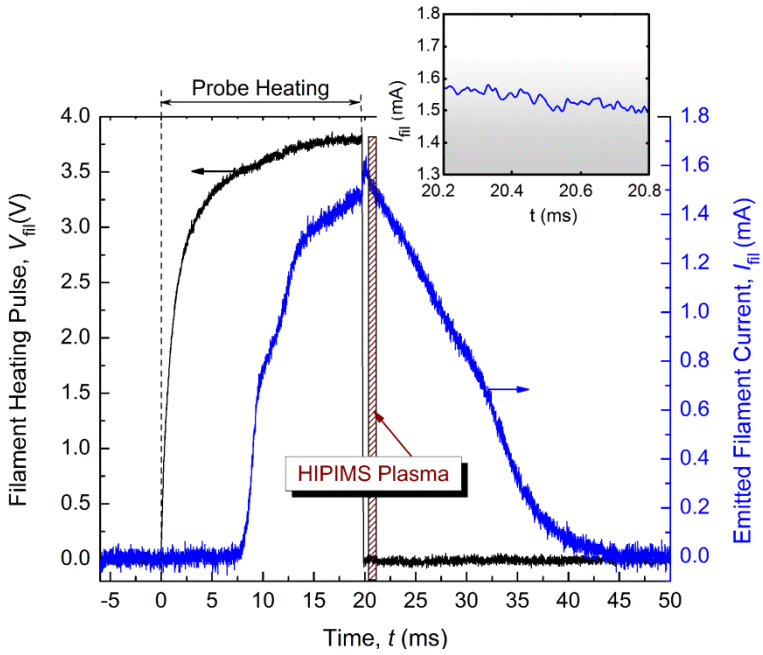

FIG. 4. (Color online) A 20 ms pulse with a peak amplitude of 3.7 V is FIG. 4. (Color online) A 20 ms pulse with a peak amplitude of 3.7 V is applied to the tungsten filament to heat it. The measurement was made differentially by placing two ground referenced probes at the positive and negative terminals of the probe. After about 10 ms, the ohmic loss in the filament has sufficiently heated it to cause electron emission. When heating is terminated, electron emission decays but at the decay rate that is sufficiently slow by comparison to a typical plasma pulse (600 µs in this case). The inset shows the decay during the plasma pulse.

III. PULSED PROBE CIRCUITRY

A schematic of the pulsing circuitry for the emissive probe is shown in Fig. 1. It consists of a transistor -transistor logic (TTL) pulse generator that synchronizes the heating with the plasma discharge, a power MOSFET, a ground-free dc heater power supply, a pulse transformer, diodes, a probe bias supply, and a current-sensing resistor. The MOSFET switches the heater power supply across the pulse transformer,

which is necessary to electrically isolate the probe so that it can assume the potential determined by the probe bias voltage (or float in the absence of bias). Diodes are employed to rectify the output pulse and prevent - *L(di/dt)* transients. When the probe is biased, a current-sensing resistor connects the common of the transformer's secondary winding to a bias voltage supply.

Given the low-voltage, low-frequency operation of this circuit, component choices are not critical. A MOSFET with a 50 V, 1 A rating is more than sufficient, but care should be taken to choose a device with small on-resistance and a package with good thermal conductivity. Since the impedance of the filament (approximately 5Ω at 3000 K) is comparable to the MOSFET's on-resistance (between 0.75 Ω and 3 Ω depending on junction temperature and gate drive), a significant amount of power is

dissipated in the MOSFET, so it must be well cooled for continuous operation. The pulse transformer needs to have sufficient mutual inductance and a high enough saturation flux density to prevent droop and/or core saturation.

The average power transferred through the transformer is typically less than 5 W, so cooling is not difficult given that the transformer will not be lossy at these relatively long time scales of the pulsing scheme. There are no special requirements to the diodes; standard 50 V, 1 A Si rectifiers are sufficient. The power MOSFET was an IRF840 500 V, 8 A; the diodes were DO-204AL 1 kV, 1 A; the ground-free heater power supply was a TENMA 72-7295 0-40 VDC, 0-3 A adjustable supply; and the probe bias supply was a KEPCO BOP72 controlled by the SIGNALEXPRESS software (we note that the circuit was built with parts and devices available in the lab, so the ratings exceed requirements in some cases).

The MOSFET's gate was driven by a TENMA TGP110 TTL pulse generator with an adjustable pulse width and repetition rate. The gate of the MOSFET was loaded with a 100 nF capacitor to slow its turn-on, which mitigates transients from switching the floating power supply to ground.

The radial position of the probe was controlled by LABVIEW SIGNALEXPRESS software driving a linear motion feedthrough with a stepper motor. The software controlled not only the positioning but synchronized the position with the measuring procedure described in the following sections. The ±10 V analog output of the NI PXIe-6341-card was amplified a factor of 10 by the KEPCO BOP72 amplifier which provided the actual probe bias voltage. By automating the measurement, including the mechanical advancement of the probe, the probe's exposure to the HIPIMS plasma was minimized and the detrimental effects (i.e., coatings) on filament's lifetime were reduced.

IV. PROBE OPERATION

Figure 4 illustrates typical waveforms for the probe's heating pulse and emitted current. This measurement was made at a base pressure of 1×10^{-4} Pa with the probe biased at -50 V. In this example, the probe is heated with about 3.7 V for 20 ms, or about 36 mJ, which, for a -50 V bias, results in a peak emitted electron current of about 1.6 mA. The most important thing to note in Fig. 4 is that the electron current collected after the heating pulse is relatively constant over the period of time during which a typical plasma discharge would occur. For a 600 µs pulse, the collected electron current only changes by 4% from 1.58 mA to 1.51 mA.

Accurate plasma potential measurements from the floating probe measurement technique require strong filament emission during the measurement period. The thermionic current density emitted from a metal is strongly temperature dependent, as described by the Richardson equation,[15]

$$J = A_G T^2 e^{-(W/(k_B T))}, \qquad (3)$$

where J is the emitted electron current density, T is the temperature, W is the metal's work function, and A_G is the Richardson constant.

Since the filament was originally designed for its usual operation in a xenon gas environment, an experiment was conducted to investigate the filament's thermal properties in a lower pressure environment, where convection cooling does not apply. Figure 5 shows the black body radiation emitted by the glowing probe in vacuum for different average powers.

The measurement was made using a spectrometer for the visible spectral range (Ocean Optics USB-4000). The spectrometer was set to have an integration time of 10 ms, and the software was set to average 100 scans and to apply boxcar smoothing with a width of 30 pixels. System losses and detector sensitivity were calibrated out of the measurements by dividing the measured data by the system's transfer function.

The transfer function was determined by heating the probe with the right amount of power, so its emission nearly matched the spectrum of an Ocean Optics LS-1 tungsten halogen light source with a filament temperature at 3100 K. Emission was then compared to the Planck distribution to obtain the wavelength-dependent system transfer function.

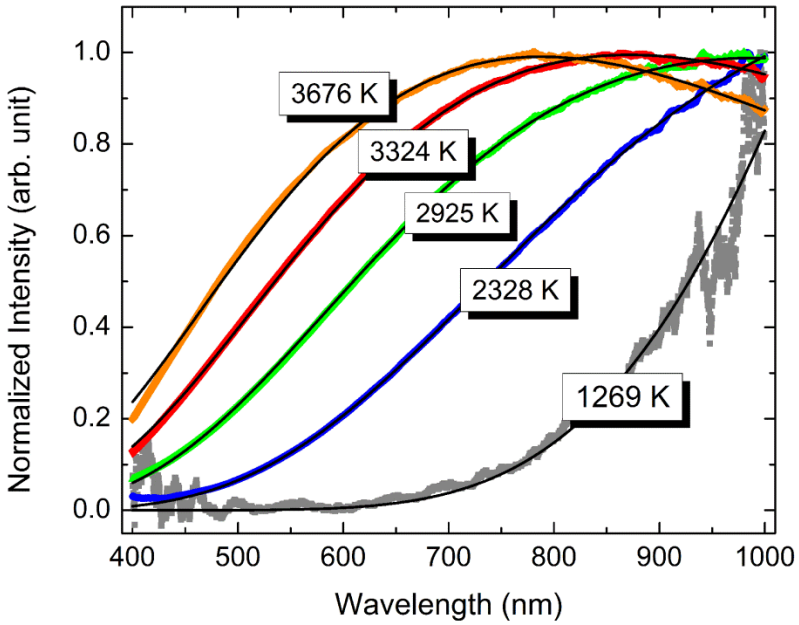

FIG. 5. (Color online) Normalized time-averaged intensity of black body radiation emitted from the hot emissive probe for different pulsed heating powers leading to different temperatures. The indicated temperature is calculated from fitting the intensity measurements (dense sequence of colored symbols) to fitting curves (black solid lines) of a black body radiator (note the emissivity is not important since we deal with normalized curves).

As expected, the absence of convection cooling results in higher filament temperature than with the usual filament's power rating. For each applied power, the filament temperature could be calculated

by fitting the calibrated measured intensity (colored data symbols in Fig. 5) with a fitted black body radiation curve (solid black lines in Fig. 5). The resulting temperatures are displayed as curve labels. We stress that the time resolution of the measurements was 10 ms, and therefore, the peak temperature of the probe could be somewhat higher than the temperature fitted to the spectral intensity curves. The validity of the temperature measurement approach was further checked by heating the filament up to the tungsten melting temperature (at 3695 K, when it stopped working, of course). Consistent with the temperatures determined by black body intensity distribution, the filament reached the tungsten melting temperate as the applied power was only 0.5 W, at a filament voltage drop of 1.75 V, corresponding to 58% of the bulb's rated dc operating voltage.

The pulsed probe operation is ultimately limited by the repetition rate of the discharges. As the duty cycle increases, the time available to heat the probe decreases and the amplitude of the heating pulse must be turned up so that the filament reaches its emission temperature sufficiently fast (Fig. 6).

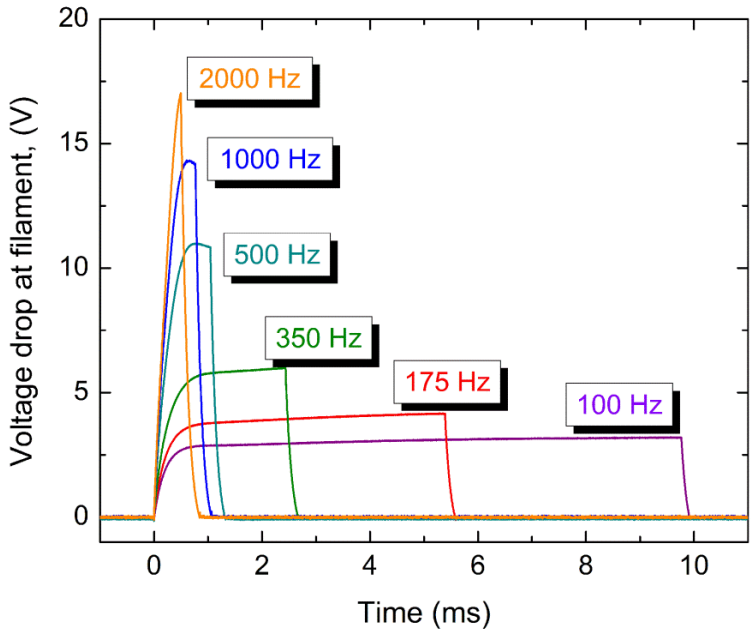

FIG. 6. (Color online) As the duty cycle increases, the duration and amplitude of the heating pulse must be decreased and increased, respectively. Higher voltage drop at the filament would imply greater measurement uncertainty and plasma disturbance, emphasizing the benefit of the pulsed approach presented here.

An upper bound on the repetition rate has not yet been determined; the probe was run with a heating time as short as 500 µs, which would accommodate repetition rates as high as 2 kHz, which is higher than the repetition rates used in many pulsed plasma processing techniques. Further investigations are required to determine how the probe's lifetime is reduced by the repetitive

thermal stress upon the many fast heating and cooling cycles. Effects like shorting by metal coating or oxidation in an oxidizing environment, if applicable, may also limit the probe's lifetime.

V. DEMONSTRATION OF THE TECHNIQUE BY HIPIMS EXPERIMENTS

Experiments to test the probe's operation were conducted in a small diagnostic chamber with a planar magnetron that was pulsed with a SPIK2000A high voltage and high power pulse generator from MELEC GmbH (maximum voltage 1 kV, maximum peak current 500 A). The electrical connections and gas feedthroughs to the chamber are shown in Fig. 3. The cylindrical stainless steel chamber with several Conflat® ports had an inner diameter of 35 cm and a depth of 25.4 cm.

It was pumped down to a base pressure of 1×10^{-4} Pa with a Pfeiffer TMH 521 turbo pump backed with an MD 4 diaphragm pump from Vacuumbrand GmbH. During the experiments, an MKS mass flow controller supplied argon, raising the pressure to 0.28 Pa or 0.33 Pa.

A 6.25 mm thick, 7.6 cm diameter Nb target was used with an unbalanced planar magnetron (US Inc.®) and HIPIMS pulses were supplied by a high current SPIK2000A pulse generator (Melec® GmbH), capable of delivering up to 500 A peak current should the plasma impedance require it. A delay generator was used to synchronize the probe heating pulses with the discharge pulses (Fig. 3). For the data presented here, the HIPIMS discharges were operated at a repetition rate of 10 pulses per second and each pulse starting 200 μs after the end of a 20 ms heating pulse.

The magnetron was pulsed with negative voltages (relative to the grounded anode) between 400 and 600 V to create a mixed argon and niobium plasma. HIPIMS (Refs. [16] and [17]) is a physical vapor deposition technique that combines pulsed power systems with magnetron sputtering to produce plasmas of the target material. The peak power exceeds the average power by typically two orders of magnitude.[18] Care must be taken when measuring the potential of magnetically confined plasmas because the motion of magnetized electrons can lead to inaccurate determinations of the potential.

The helical motion of magnetized electrons is described in part by the particle's Larmor radius, given by

$$r_L = \frac{m_e v_\perp}{eB}, \qquad (4)$$

where m_e is the electron mass, $v_\perp$ is the component of the electron's velocity perpendicular to the magnetic field, e is the charge of the electron, and B is the magnetic field. If the Larmor radius is smaller than the probe's radius, emission from the probe reduces because a fraction of the electrons will return

to the probe.[10] Measurements of the potential have been made with the probe positioned between 15 and 30 mm away from the target, which corresponds to magnetic field strengths between 42 and

8 mT, above the racetrack, as measured with a Hall probe (F.W. Bell, Inc.). Assuming an electron temperature

of 2 eV, which is approximately the temperature of the lower energy electrons in the non-Maxwellian plasma,[11] this corresponds to minimum Larmor radii between 120 μm and 600 μm, which are, respectively, 8 and 40 times larger than the probe's radius. For positions closer than 20 mm to the target, the cathode voltage required to ignite the plasma increased, indicating that electrons emitted from the probe were perturbing the discharge. Inside of 15 mm, electron emission prevented plasma ignition completely, presumably because the physical presence of the probe interferes with the closed

drift (Hall) current. Therefore, the measurements presented here to illustrate the principle were taken at a distance of 30 mm from the target.

VI. RESULTS OF TEST EXPERIMENTS

As is typical for HIPIMS discharges with constant voltage drive during the pulse, the power varies significantly depending on the operating pressure, cathode pulse amplitude, pulse width, and duty cycle. Figure 7 illustrates two different discharge modes: in the low power mode, we see the discharge settle to what would essentially be dc operation if the discharge were not terminated. In the high power mode,

the current runs away, more than an order of magnitude higher than the low power current, upon a relatively small increase in discharge voltage. The mode of discharge is altered by adjusting the applied HIPIMS voltage and the Ar pressure: in this case from 400 V and 0.28 Pa for the low power mode to 420 V and 0.33 Pa for the high power mode. The strong sensitivity of the discharge current on the applied

voltage (and other parameters like Ar pressure and magnetic field) is an expected discharge runaway feature which has been discussed in the literature.[17–19]

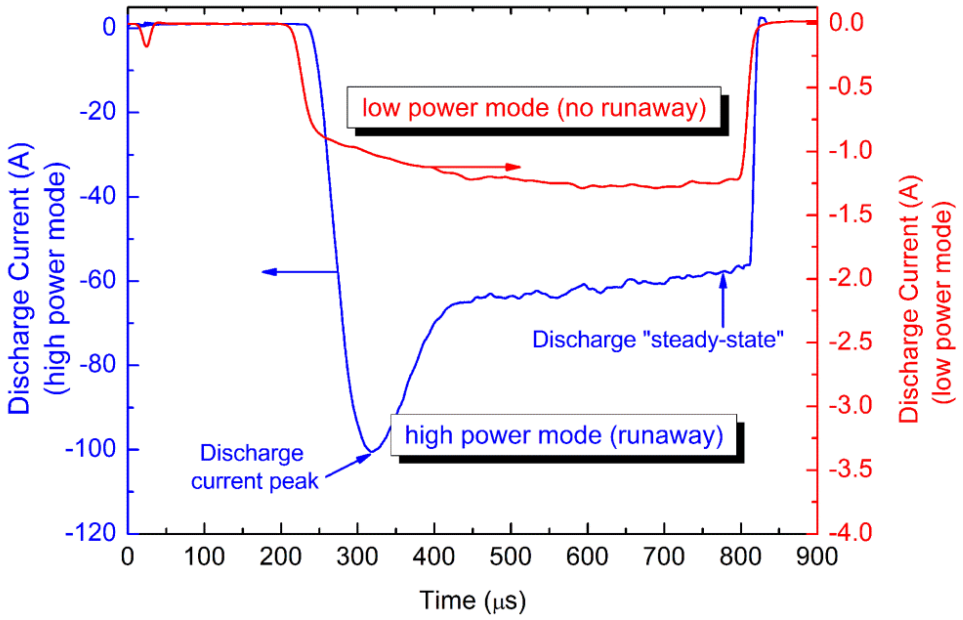

FIG. 7. (Color online) Examples of current pulses for low and high power modes: the low power mode is shown here with -400 V applied to the Nb cathode for 800 μs at 0.33 Pa; the high power mode was observed by increasing the discharge voltage to -420 V at an argon pressure 0.28 Pa; in both cases, the repetition rate was set to 10 pulses per second. Note that the current scale for the low power mode was increased by a factor 30, compared to the high power mode, to better show the current shape. Time zero is defined at the time when the voltage is applied to the target.

To measure the plasma potential, the probe bias voltage is swept over a wide range and the probe current is plotted versus the bias voltage. The saturated probe technique takes the plasma potential as the probe potential where the probe current intercepts the bias voltage axis (the emitted and received

currents are equal). Fig. 8 shows a typical current-voltage characteristic of a cold probe and a heated, emissive probe.

For this measurement, -400 V pulses were applied to the Nb target 200 μs synchronized after 3.7 V pulses were applied to the filament for 20 ms. The repetition rate was set to 10 pulses per second. The probe current in the I-V curve is the time-average of current measured across the current sensing resistor for a 200 μs time period in the steady-state part of the discharge waveform, as depicted in Fig. 7. As the bias is swept from -80 to 80 V, the current measured via the current sense resistor shown in Fig. 8 exhibit the expected response for the cold and hot (emissive) probe conditions.

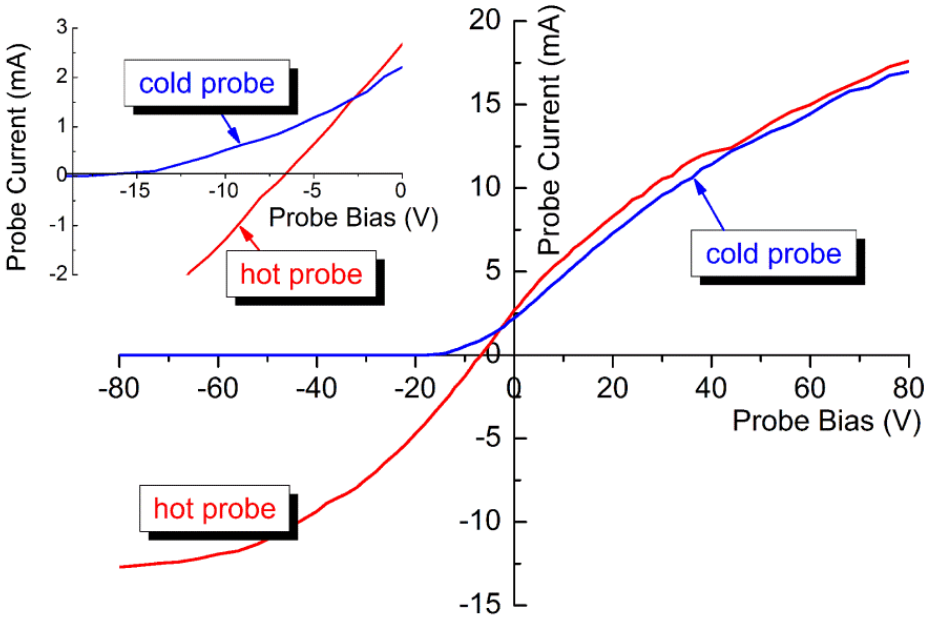

FIG. 8. (Color online) The probe's bias was swept twice: once with heating pulses applied to the probe, once without. The measurements with the hot probe indicates a plasma potential of approximately −7.8 V at a distance of 20 mm from the target.

The *I-V* characteristic of the cold probe shows a small ion saturation current (left side of the characteristic) and a much greater electron current (right side), a well-known consequence of the significantly different mobility of ions and electrons due to their mass difference. Under our conditions, the floating potential of the cold probe is about -16 V. As explained in conjunction with Eq. (2), the floating potential shifts to more positive values, approaching the plasma potential, when the probe is heated and the electron emission is sufficiently high.

When a voltage pulse of -420 V is applied to the target, the discharge took about 200 µs from the start of the pulse for the plasma to ignite, see Fig. 7. However, the delay time decreased with increasing pulse voltage, as known from the literature.[20] One sees the initial discharge current peak followed by rarefaction and steady-state phase with a discharge current of about 60 A.

By monitoring the probe current during different phases of the discharge as a function of the applied probe bias voltage, the plasma potential at different times and discharge intensities can be quantified. Here, we choose two distinctive points, namely, the plasma potential at the discharge peak and at the end of the discharge pulse where we observe near-steady- state plasma. As discussed above, the plasma potential was defined as the voltage at zero probe current. Graphically, it is the point where the probe current crosses the dashed horizontal line as depicted in Fig. 9.

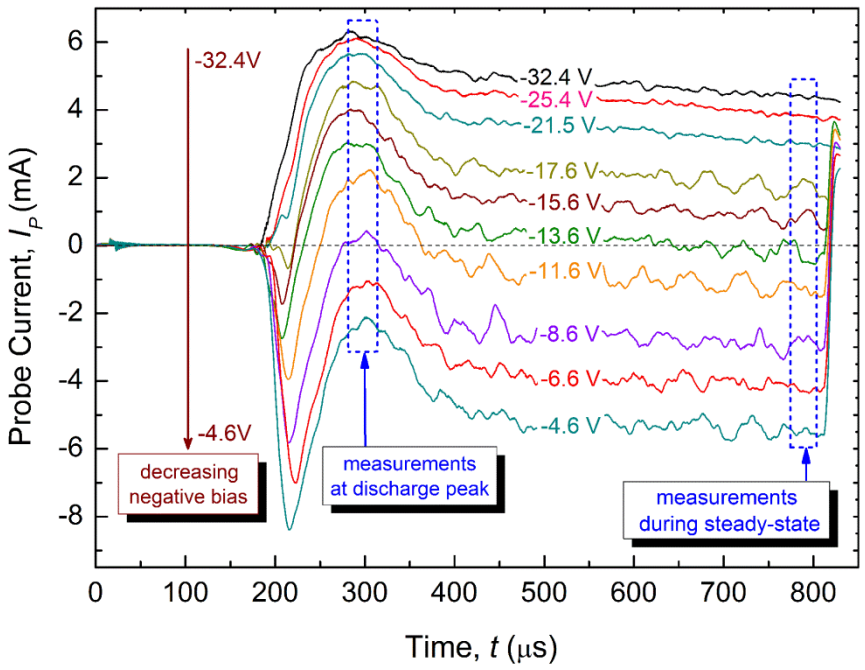

FIG. 9. (Color online) Probe current I_P as a function of time during the pulse for a given applied bias voltage V_B; the probe was positioned at r = 2 mm, z = 30 mm.

The initial time-resolved probe measurements reported here were made by sweeping the bias voltage between -35 V and +5 V in 1 V steps, with the probe current readings per bias voltage step averaged over 10 pulses. By time-averaging portions of the probe current shown in Fig. 9, it is possible to reduce the data to show how the probe current varies with bias at different times of the discharge. Figure 10 illustrates the dependence of probe current on bias voltage at both the discharge peak and the steady state, as defined in Fig. 9. Plotting the data in this fashion is useful because it simplifies the process of identifying the plasma potential at different phases of the discharge.

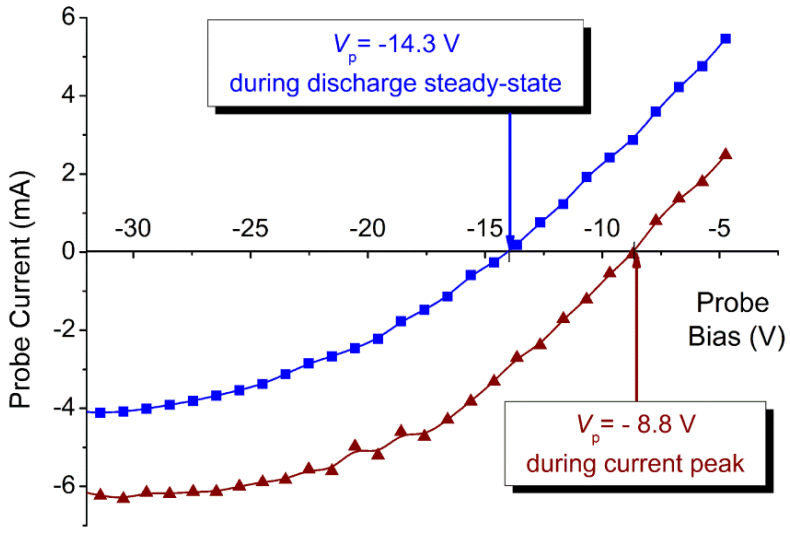

FIG. 10. (Color online) I-V characteristic of the emissive probe, the probe was positioned at r = 2 mm from the target axis, and z = 30 mm from target surface. Bias sweeps are shown for two different phases of the discharge, the peak current, and steady-state current, as indicated in Fig. 8.

Figure 11 shows the radial plasma potential distribution. Towards the center of the magnetron, V_{Pl} is rapidly increased to values of -10 V, and we observe about -30 V in region of the target's racetrack, where the electrons are trapped by the magnetic field lines. The investigations, thus, showed that the radial plasma potential distribution is strongly dependent on the local magnetic field strength. Much more detailed measurements of the plasma potential distribution will be reported in the near future.

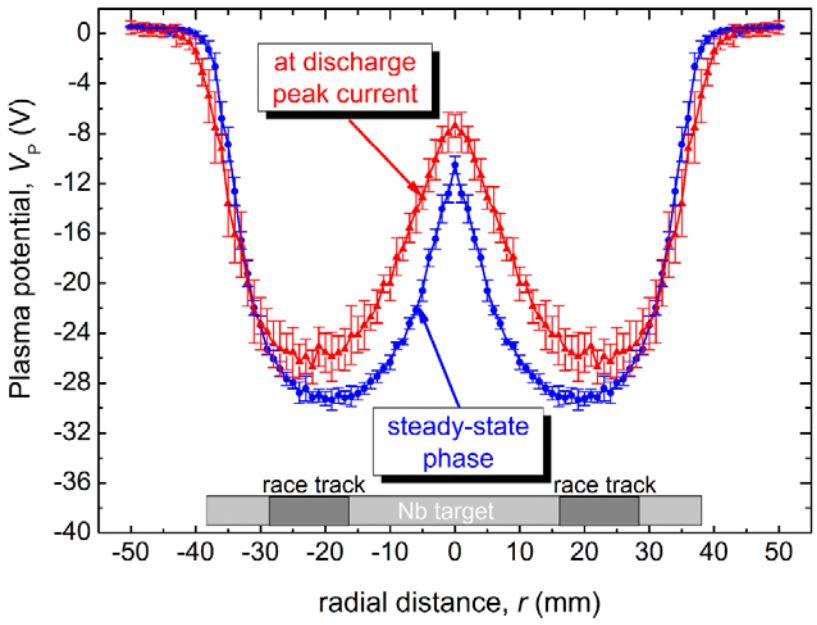

FIG. 11. (Color online) Plots of the plasma potential versus the radial distance *r* to the center of the magnetron. The probe position was 30 mm in front of the target. The measurement was performed over half the target (from 0 mm to 46 mm) and mirrored to facilitate understanding. The error bars indicate the standard deviation.

VII. CONCLUSIONS

In summary, we have demonstrated that an emissive probe can be constructed and operated under pulsed conditions, and applied to transient plasmas like those created by HIPIMS. Alternating heating and plasma production has the advantage that the voltage drop along the heated filament is practically zero during the measurements, which removes any uncertainty regarding perturbations to the plasma by an electric field across the filament. Additionally, we do not need to worry about the magnetic field that is produced by the heating current, especially when the heated filament has a shape of a small coil, as in this study. The coil shape is convenient since filaments from commercial miniature light bulbs could be used at a fraction of the cost of building or replacing custom probe filaments. The temperature and electron emission from the pulsed emissive probe were measured optically and electrically, respectively, indicating sufficient thermal inertia that the emission of electrons can be considered almost constant during the plasma pulse. Pulsed emissive probe operation was demonstrated by measuring the plasma potential distribution 30 mm from a niobium target under HIPIMS conditions. The results shown here indicate a potential drop of about -30 V in front of the racetrack region. This voltage drop is associated with the magnetic presheath, while most of the anode-cathode voltage drop is located in the thin (mm) sheath next to the target surface. Further measurements with this technique will reveal the complete potential distribution by positioning the emissive probe at positions of interest in the axial and radial directions.

ACKNOWLEDGMENTS

We gratefully acknowledge help by Dr. S. Lim and J. Wallig for assistance in probe construction and vacuum technology. A. Rauch thanks the Austrian Marshall Plan Foundation (www.marshallplan.at) for funding a scholarship.

J.M. Sanders thanks the AFOSR for supporting his Ph.D. research. This work was done at Lawrence Berkeley National Laboratory with support by U.S. Department of Energy under

Contract No. DE-AC02-05CH11231.

VIII. REFERENCE

[1]A. Y. Wong, G. Dimonte, J. R. Ferron, M. Y. Fukao, K. Jones, A. Kuthi,K. L. Lam, B. J. Leikind, R. W. Schumacher, H. Stephanian, and R. G. Suchannek, Nucl. Instrum. Methods Phys. Res. 207(1–2), 207 (1983).

[2]R. Schrittwieser, R. Adamek, P. Balan, M. Hron, C. Ionita, K. Jakubka, L.Kryska, E. Martines, J. Stockel, M. Tichy, and G. Van Oost, Plasma Phys.Controlled Fusion 44(5), 567 (2002).

[3]N. Mahdizadeh, F. Greiner, M. Ramisch, U. Stroth, W. Guttenfelder, C.Lechte, and K. Rahbarnia, Plasma Phys. Controlled Fusion 47(4), 569(2005).

[4]I. Langmuir, Phys. Rev. 22(4), 357 (1923).

[5]Y. E. Wang, T. Intrator, and N. Hershkowitz, Rev. Sci. Instrum. 56(4), 519 (1985).

[6]R. F. Kemp and J. M. Sellen, Jr., Rev. Sci. Instrum. 37(4), 455 (1966).

[7]P. Balan, R. Schrittwieser, C. Ionita, J. A. Cabral, H. F. C. Figueiredo,H. Fernandes, C. Varandas, J. Adamek, M. Hron, J. Stockel, E. Martines,M. Tichy, and G. Van Oost, Rev. Sci. Instrum. 74(3), 1583 (2003).

[8]G. D. Hobbs and J. A. Wesson, Plasma Phys. 9(1), 85 (1967).

[9]J. R. Smith, N. Hershkowitz, and P. Coakley, Rev. Sci. Instrum. 50(2), 210(1979).

[10]J. W. Bradley S. Thompson, and Y. Aranda Gonzalvo, Plasma Sources Sci.Technol. 10(3), 490 (2001).

[11]A. Mishra, P. J. Kelly, and J. W. Bradley, Plasma Sources Sci. Technol.19(4), 045014 (2010).

[12]W. E. Yao, T. Intrator, and N. Hershkowitz, Rev. Sci. Instrum. 56(4), 519(1985).

[13]H. Shindo, M. Konishi, and T. Tamaru, Rev. Sci. Instrum. 59(9), 2002(1988).

[14]U. Helmersson, M. Lattemann, J. Bohlmark, A. P. Ehiasarian, and J. T. Gudmundsson, Thin Solid Films 513(1–2), 1 (2006).

[15]A. Anders, Cathodic Arcs: From Fractal Spots to Energetic Condensation (Springer-Verlag, New York, 2008).

[16]V. Kouznetsov, K. Macák, J. M. Schneider, U. Helmersson, and I. Petrov, Surf. Coat. Technol. 122(2–3), 290 (1999).

[17]A. Anders, J. Andersson, and A. Ehiasarian, J. Appl. Phys. 102(11), 113303 (2007).

[18]A. Anders, Surf. Coat. Technol. 205(Supplement 2), S1 (2011).

[19]J. Vl˘cek and K. Burcalová, Plasma Sources Sci. Technol. 19(6), 065010 (2010).

[20]G. Y. Yushkov and A. Anders, IEEE Trans. Plasma Sci 38(11), 3028 (2010).

J. Appl. Phys., to be submitted (2011)

Spatial and temporal investigation of high power magnetron discharges by 2D electric probe mapping

Albert Rauch,[1] Rueben J. Mendelsberg,[1] Jason M. Sanders,[1,2] and André Anders[1,]

[1]*Lawrence Berkeley National Laboratory, University of California, Berkeley, California 94720, USA*

[2]*Department of Electrical Engineering, University of Southern California, Los Angeles, California 90089, USA*

Pulsed emissive probe techniques have been used to determine the spatial plasma potential of high power impulse magnetron sputtering (HiPIMS) discharges with high spatial and temporal resolution. HiPIMS discharges with a 76 mm niobium target in 0.26 Pa argon were investigated for pulse widths of 100 µs at a pulse repetition rate of 100 pulses per second; the average power was set to 240 W. Time resolution of 20 ns and a spatial resolution of 1 mm were achieved. It is shown that the plasma potential varies greatly in space and time, with the lowest potential over the target's racetrack. The magnetic presheath exhibits a relatively strong, non-uniform electric field, derived from $\mathbf{E} = -\nabla V_p$, accelerating ions formed in the presheath toward the racetrack. The electron's $\mathbf{E} \times \mathbf{B}$ drift was determined based on the knowledge of the local $\mathbf{E}$ and static $\mathbf{B}$ fields. Very significant local variations were found, which support the growing evidence in the literature that the HIPIMS plasma exhibit structures and is subject to waves and instabilities.

I. INTRODUCTION

High Power Impulse Magnetron Sputtering (HiPIMS) is an increasingly used ionized physical vapor deposition (i-PVD) technology that combines magnetron sputtering with pulsed power technology. In contrast to conventional magnetron sputtering it provides greater opportunities to engineer the microstructure and improve the quality of thin films by utilizing the kinetic and potential energies of ions of the target material [1, 2].

High power pulses with a length of typically 50-500 µs are applied to a conventional planar magnetron. To keep the average power well within the power specifications of the magnetron, the HIPIMS process is done with low duty cycle and repetition rates less than 1 kHz. Special power supplies have been developed and are today available from several vendors; they feature high peak currents and fast arc suppression circuits. The power density, averaged over the target area, can reach, and occasionally even exceed, 10^7 W/m². As a result, plasma densities of order 10^{19} m^{-3} in front of the target are not uncommon [3]. Sputtered atoms traveling from the target surface pass through the dense plasma and are likely to become ionized and thus participate in the sputtering process [2, 4]. The discharge currents in the HIPIMS process can often reach hundreds of amperes. The current and other parameters depend on the applied voltage, gas pressure, magnetic field strength, and the target's material, size, and surface conditions.

Magnetrons are characterized by a closed-drift of electrons: the large azimuthal Hall current, primarily caused by the $\mathbf{E}\times\mathbf{B}$ drift of electrons, typically exceeds the discharge current by a factor of 3-9 for direct current (dc) conditions [5]. This factor is smaller for HIPIMS conditions [3], which can be associated with "anomalous" current transport across magnetic field lines based on collective processes (oscillations and instabilities). The non-uniformities of the electric and magnetic fields give rise to additional drifts, for example the magnetized electrons also experience $\mathbf{B}\times\nabla\mathbf{B}$ and higher order drifts. Lundin *et al.* explained the anomalous electron transport by fast (MHz) oscillations in the electric field in the azimuthal direction as observed with probes [6]. HiPIMS plasmas contain counter-streaming fluxes of ions, electrons and neutrals, all in the presence of a magnetic field, and therefore one should expect a whole variety of waves and instabilities.

Mapping magnetic and electric fields with good time and spatial resolution is desirable in order to gain a deeper understanding of the HIPIMS discharge in general and its instabilities in particular. For the present work we picked a relatively simple situation: HIPIMS discharges with constant-voltage pulses using a transition metal (Nb) target operating in a noble gas. The experiments will show rather non-form field distributions even as we do not simultaneously resolve potential measurements in space and time. Rather, the results were obtained from about 10^6 HIPIMS pulses,

presenting a total of several 10^9 individual data points, enabled by semi-automated digital recording technology.

II. EMISSIVE PROBE TECHNIQUES

Before we go into the details of the experiments and results, it seems appropriate to very briefly recap plasma probe techniques, and in particular emissive probe techniques, as applied to HIPIMS discharges. Not surprisingly, HIPIMS plasma has been extensively studied using Langmuir probes[7-9]. Various levels of time resolution have been demonstrated for selected positions of the probe, mostly focusing on the interesting region above the racetrack. However, measurements generally lack the survey character that would allow us to gain greater insights.

Langmuir probes are a standard diagnostic for making density and temperature measurements in plasma. In principle, the plasma potential V_p can be determined using a conventional (cold) Langmuir probe via

$$V_p = V_f + \frac{kT_e}{e\,\overline{Q}} \ln\left(\frac{I_{es}}{I_{is}}\right) \tag{1}$$

where V_f is the floating potential (the potential of the probe when the probe current is zero), T_e is the electron temperature, k is the Boltzmann constant, e is the elementary charge, $\overline{Q}$ is the mean charge state number of ions arriving at the probe (in most cases, $\overline{Q}=1$ is reasonable assumption), I_{es} and I_{is} are the electron and ion saturation currents, respectively. As it is clear from (1) that this technique requires knowledge of the electron temperature, which can fluctuate during the measurement, and the saturation currents, which in principle can be taken from the probe characteristic. However that is not always simple since small probes do not clearly show electron saturation even for quiescent plasmas due to the voltage dependence of the probe's sheath, i.e. the effective collecting area. Furthermore, relation (1) was derived assuming that the plasma electrons have a Maxwell distribution, which is not the case when a magnetic field is applied. The approach inherently has great errors whenever the plasma is not quiescent. In strongly fluctuating plasmas it is difficult to determine the characteristic knee in the currrent-voltage characterisitc that indicates the onset of electron saturation, and therefore it may be impossible to obtain satisfactory values for the plasma potential.

Emissive probes are superior and widely used when it comes to the determination of the plasma potential [8, 10, 11]. As the name suggests, an emissive probe is sufficiently hot to emit electrons via the

thermionic emission mechanism, where the current density is approximately described by the Richardson-Dushman equation:

$$j_{thermionic} = A_R T^2 \exp\left(-\frac{\phi}{kT}\right), \tag{2}$$

where $A_R = 4\pi e m_e k^2 / h^3 = 1.202 \times 10^6 \ \mathrm{A/m^2K^2}$ is the universal Richardson constant, and ϕ is the work function of the metal (about 4.5 eV for tungsten). The current measured as a function of probe bias for the emissive probe diverges from that measured for a collecting-only probe when the bias voltage is less than the plasma potential: the emitted electrons leave the probe and thereby cause an additional current. In opposite case, when the probe potential is positive with respect to the plasma potential, emitted electrons return to the probe. Therefore, one obvious way of determining the plasma potential is to find the potential where the emissive (hot) and collecting-only (cold) probe characteristics merge.

When the emission of the probe is increased by increasing the probe's heating current, the probe's floating potential shifts toward the plasma potential. This becomes clear when considering the generalization of (1) for the emitting probe by appropriately adding the emitted electron current I_{em} to the current balance (emitted electrons are electrically equivalent to collected ions)[12]:

$$V_p = V_f + \frac{kT_e}{eQ} \ln\left(\frac{I_{es}}{I_{is} + I_{em}}\right). \tag{3}$$

Eq. (3) shows that for increasing I_{em} (according to the Richardson´s emission law), the second term decreases, while the floating potential V_f of the probe approaches V_p. The second term vanishes for $I_{em} = I_{es} - I_{is}$ and then $V_p \to V_f$

If the probe temperature respectively the emission of electrons is further increased, part of the emitted electrons will be reflected by the plasma, keeping the probe at the plasma potential. The plasma potential can therefore be obtained from the floating potential of the emissive probe once it is known that the emission current is sufficiently high. We will later show that this is the case for our setup. As a consequence of its direct readout, the floating emissive probe is capable of following fast changes in plasma potentials. The floating potential can be aquired with high time resolution, using an oscilloscope. The space resolution is limited by the size of the probe including its sheath, and practically a resolution of 1 mm has been demonstrated .[13]

Emissive probes have been successfully applied when to measure plasma potentials in a wide range of magnetic fields, ranging from 10s of mT for a quadpoloe device [14] to 0.5 T at the edge of a Tokamak [12] or *Q*-machine [11].

It should be noted that the emitted electrons have energies of about 0.3 eV, corresponding to a wire temperature of $T_w \approx 3000\ \mathrm{K}$. This limits the voltage resolution of the emissive probe to about 0.3 V, which is generally not of concern given the errors of the potential measurements resulting from other factors.

Among those other factors is that the heating current of the probe's wire loop or filament is driven by a voltage, which can be undesirably high, e.g. a few volts[11]. That is, one side of the filament has a potential a few volts higher than the other due to the voltage drop, caused by the heating current. In our previous work we have introduced a pulsed version of an emissive probe addressing this issue: heating and measuring intervals alternate[15]. The probe is sufficiently hot and electron-emitting when the measurement is done, while the voltage driving the heating current is only applied in the pause between measurements. While our previous work[15] offers further details of the pulsed probe's circuitry and a discussion on emissive probe principles, we present here extensive measurements related to HIPIMS plasmas using a niobium target in argon.

III. EXPERIMENTAL DETAILS

The experimental setup and the region of probe measurements are schematically presented in Fig. 1. In the following we describe the various components of the system.

The 35 cm diameter and 25cm height stainless steel vacuum chamber was pumped with a 550 l/s turbomolecular pump (Pfeiffer TMH 521, backed by diaphragm pump) to a base pressure of about 10^{-5} Pa. High purity argon was introduced by a mass flow controller (MKS, max. flow 100 sccm). Throughout all experiments, the argon flow rate was kept at 36 sccm. The combination of flow and pumping speed gave a pressure of 0.26 Pa as recorded by a capacitance manometer (Baratron by MKS).

The planar magnetron was operated with a 6.25 mm (1/4") thick, 76 mm (3") diameter niobium target surrounded by a grounded anode ring mounted flush with the target surface. Due to the magnetic target mount no mechanical clamp ring is needed therefore the probe tip could scan the whole target area. The magnet assembly of the magnetron consists of a central magnetic cylinder and a outer magnetic ring located under the powered target electrode. This setup is typical for the required dome-shape of the magnetic field, leading to a torus-like dense plasma region whose projection onto the target surface produces the "racetrack" (zone of strongest sputtering). Due to the axial symmetry of the setup including the magnetron's magnetic field, the probe position and probe data can be decribed using cylindrical (*r,z*) coordinats. The magnetic field strength in axial and radial directions, $\mathbf{B}_z$ and $\mathbf{B}_r$ respectively, were measured with an accuracy of about 1% using a F.W

Bell 5180 Gaussmeter. The meter's probe tip was mounted on the movable arm later used for the emissive probe motion. The magnetic field was measured in the absence of the discharge. Therefore the magnetic field generated by the discharge and Hall (closed drift) currrents are not considered here.

The HiPIMS discharge was fed by a HIPIMS generator model SPIK2000A by Melec GmbH capable of delivering pulses up to 1 kV, up to 500 A, with freely adjustable duration greater than 5 µs and a repetition rate of up to 50 kHz. A Pinnacle DC power supply (1kV, 5 kW, by Advanced Energy) was used to charge the capacitors of the SPIK pulser. The actual repetition rate was set to 100 pulses per second to limit the average power delivered to the magnetron to 240 W. The pulser was operated in "unipolar negative" mode with the on-time set to 100 µs. The nominal peak power density, averaged over the total target area, reached $1.82 \cdot 10^7$ W/m². No power was applied during the off-time between pulses. The anode was grounded and all signals were recorded using ground as the reference potential.

The discharge current was inductively recorded using a current transformer (Pearson model 101, sensitivity 0.01 V/A, bandwidth 0.25 Hz-4 MHz). The discharge voltage was measured at the power feedthrough to the target using a 100x high voltage probe (Tektronix P5100). To impede fast high-amplitude oscillation that could damage the SPIK pulser, both output cables were wound three times through a ferrite ring before being connected to the target feedthrough (minus) and chamber ground (plus). All electrical signals were recorded with National Instruments PXI-5105 high speed Digitizer/Oscilloscope with up to 60 MS/s real-time sampling rate per channel, operated under a LabView Signal Express program.

The probe was aligned in axial direction, as indicated in Fig. 1, and radially scanned from r = 0 mm up to r = 38 mm from the center in Δr = 1 mm steps. Then the axial position of the magnetron was changed and the next radial scan of the probe executed without having to break vacuum. The axial positions covered the range from z = 1 mm near the target to z = 72 mm relatively away from it. The increasing steps are depicted by the position of the grid points in Fig. 1. The step size was set to Δz = 1 mm from 1 mm ≤ z ≤ 20 mm, and increased to Δz = 2 mm from 20 mm ≤ z ≤ 40 mm, and to Δz = 4mm from 40 mm ≤ z ≤ 72 mm, defining a measurement grid of 39×38=1482 locations. The such-defined region covers most of the target presheath and includes a typical substrate position. However, even as the probe tip can reach all those locations, not all of them can be used because the probe greatly disturbs the plasma if brought too close to the racetrack. The closest approach of the probe to the racetrack was 15 mm. Upon closer insertion, ignition of the HIPIMS pulses was hindered, presumably because the physical presence of the probe interferes (intersecting the closet

magnetic flux) with the closed drift (Hall) current and cause a large decrease in the discharge current. This limitation (lack of data near the racetrack) will be visible when we present the results.

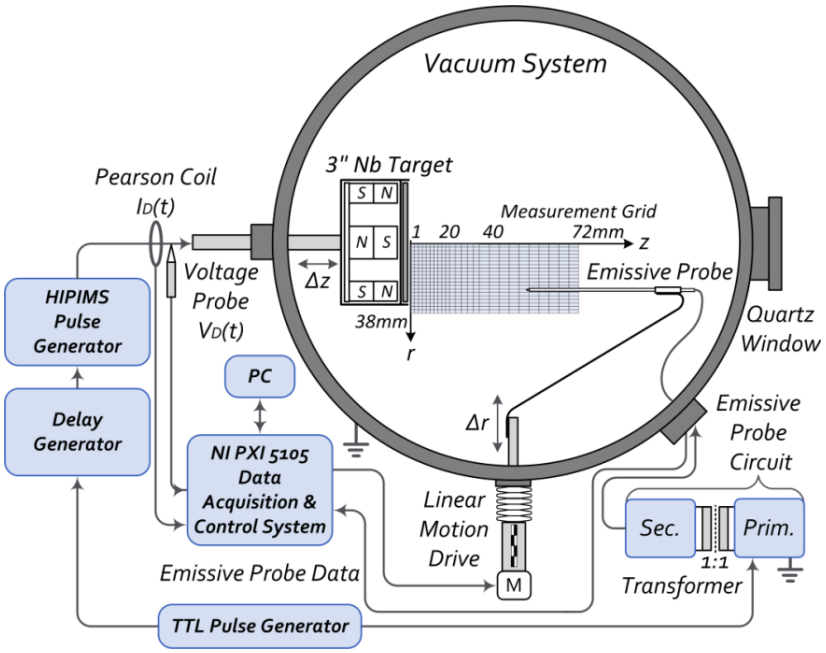

Figure 1 Experimental setup showing the arrangement and basic circuitry of the magnetron and probe diagnostics.

The emissive probe used for this experiment consists of a ceramic tube (Al_2O_3) with an outer diameter of 1.57 mm and a length of 140 mm. The ceramic tube has two bores of 0.41 mm diameter, through which a 75 µm diameter wire is inserted in such a way that on one side of the tube the tungsten wire loop of 1.5 mm diameter is formed.

Inside the bores the tungsten wire is spliced with thin copper threads (diameter 50 µm) to increase the conductivity. The contact is further improved by the roughness of the tungsten wire and the softness of the cooper. This guarantees that only the exposed probe loop is heated when a current is passed through the probe wire. Electrical connection to the probe was made through the protruding copper wires and electrical feedtrough. The cold-state electrical impedance between the two probe connectors was 0.78 Ω, in heated operation the resistivity increase to 1.91 Ω. The plane of the probe loop is directed parallel to the magnetic field lines to minimize the influence on the plasma.

Ohmic heating of the probe wire was achieved by a pulsed current triggered out of phase with the HIPIMS discharge pulse as explained in our previous work [Sanders, 2011 #7051]. The probe was made floating by sending the heating current through a 1:1 isolation pulse transformer. The potential of the floating emissive probe was acquired using an attenuating (100x) voltage probe

(Tektronix P5100, 100 MΩ input impedance, 10 MHz bandwidth) connected to the NI PXI 5105 data acquisition system. In order to suitably synchronize probe heating pulse and HIPIMS discharge pulse, an external TTL pulse generator (TENMA TGP110) was used as the experiment's clock; it provided a signal to the heating circuit and also triggered a delay generator (Tektronix PG508) which was connected to the external gate input of the SPIK pulser.

To improve the signal to noise ratio, each time resolved measurement at a given probe location was repeated 100 times for the same discharge conditions, and an average could be produced showing a standard deviation of only ±0.4 V in the relatively quiescent plasma of $z > 30$ mm and about ±3 V near the target, which coresponds to about 4% and 5-8% of the measured plasma potential values, respectively.

Gudmundsson et al [16] have measured the electron energy distribution, resolved in time and space. They found that the electron temperature is only *0.5 - 2 eV*. However, it is expected that the average electron energy is much higher (1-2 orders of magnitude), in a close location to the target surface. The magnetic field in our case at *r=15 mm* is *B = 21 mT*, which leads to an electron Larmor gyro radius of $r_L = (2 \cdot T_e \cdot m_e)^{1/2}/(e \cdot B) \approx 227\mu m$, assuming an electron temperature of *2 eV*. Thus the probes filament size fulfilled the basic requirements of the Langmuir probe diagnostics, since the probe radius r_P*=37.5 μm* is smaller than the Larmor radius of the emitted electrons.

The radial position of the probe was controlled by LabView Signalexpress software driving a linear motion feedthrough system with a stepper motor. The software controlled not only the positioning but synchronized the position with the plasma potential measurements. Data analysis and visualization was carried out using custom MATLAB scripts.

III a. Magnetic field measurements

Figure 2 (top) shows the measured magnetic field distribution in the r-z plane. The vector arrows are normalized and indicate the direction of the magnetic field B, while the conturplot shows the magnitude of $|\mathbf{B}| = \left(B_r^2 + B_z^2\right)^{1/2}$. This measurements would represent the entire information for the discharge volume if perfect axial symmetry of the magnetron could be assumed. As the bottom part of Fig. 2 shows, there are quite noticable deviation from symmetry.

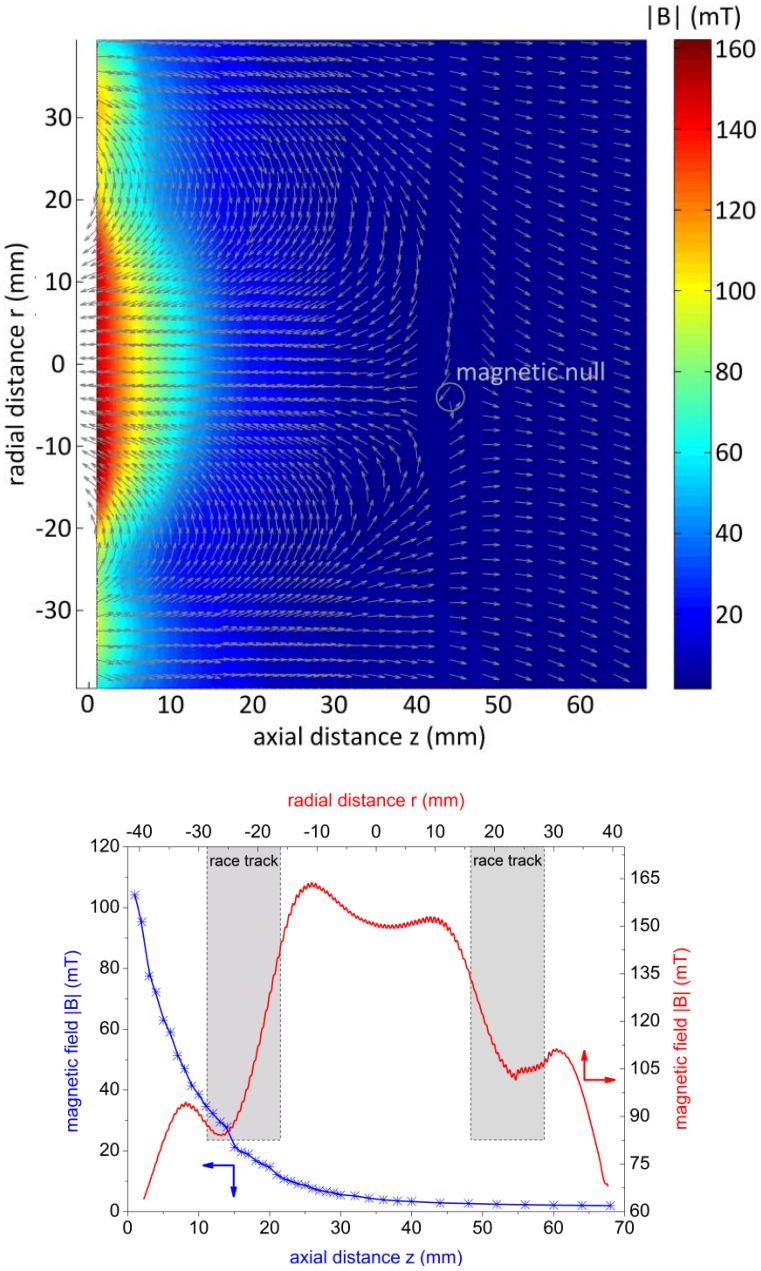

Figure 2 top: Measured magnetic field and field line directions for the magnetron used; bottom: Dependence of the magnetic field |B| on an axial line above the racetrack at r = 24 mm (blue), and |B| in radial direction at z =1 mm (red).

The "magnetic null" was found at z = 44 mm away from the center of the target slightly out of the center line. The magnetic trap indicates the extent of the magnetic presheath, the outermost magnetic field defining the zone of confinded electrons and thus the zone of densest plasma. A magnetic null point so close to the target indictes that we deal with a very unbalanced magnetron, which is confirmed by the presence of field lines guiding plasma away from the magnetron. Field lines about parallel to the target surface define the racetrack, in our case for a radius 16 mm < r < 28 mm.

III b. Emissive probe signals

The first step of the experiment focused on correct timing of pulses and sufficient electron emission during HiPIMS pulsing. Fig. 3 shows the waveforms for the probe's heating voltage pulse V_{FIL} with the associated filament heating current I_{FIL}, the emitted electron current I_E, and the external gate pulse V_T for one HIPIMS pulse. The electron emission current after the heating pulse decays relatively slowly, which ensures that emission is practically constant during the HIPIMS pulse, as depicted in the inset of Fig. 3. The electron emission current changes from 2.115 mA to 2.080 mA during the HIPIMS pulse on time, corresponde to only 1.6%.

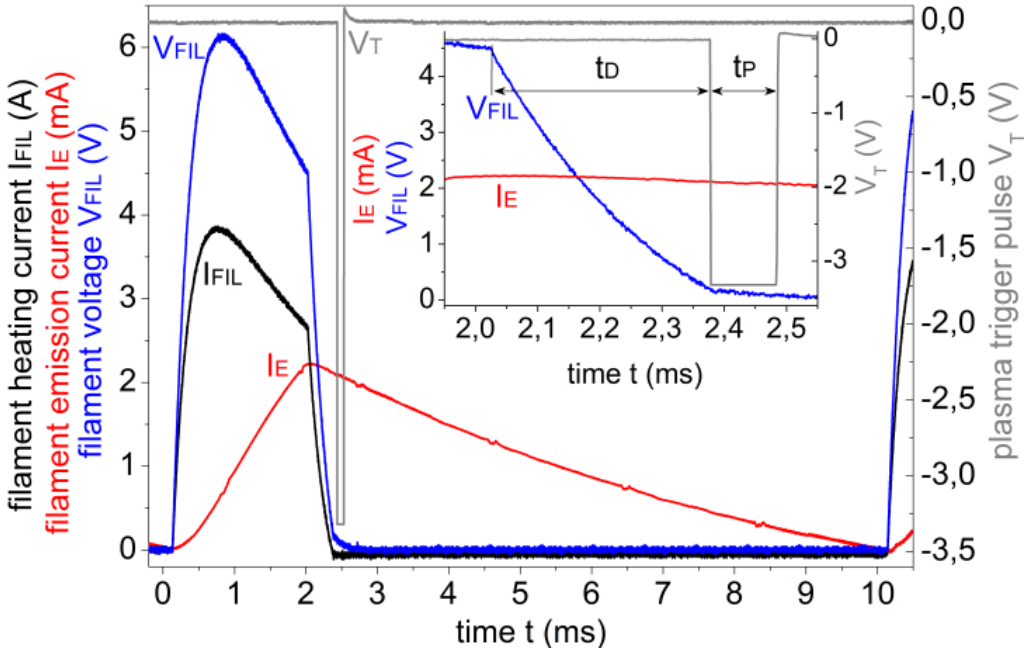

Figure 3 A 1.9 ms, 6 V peak pulse is applied to the tungsten filament to heat it. At 2.1 ms, the heating is terminated but electron emission continues well beyond the end of the HIPIMS pulse; t_D = 350 µs indicates the delay between termination of heating and application of the HIPIMS target voltage, and t_P = 100 µs is the duration of the applied HIPIMS pulse voltage.

In order to ensure the emitted current is sufficient, one can look for the change of the floating potential with increasing emission (filament temperature), as governed by equ. (3). Fig. 4 shows the measured floating potential as a function of the heating current for two different positions in front of the target. The graph is composed of many data points, each point recorded for one HIPIMS pulse at nominally the same discharge conditions. At first, when the probe is not or not sufficiently heated, the floating potential is about -17.5 V, respectively -47 V. An increase can be observed when the heating current reaches 1.0 A, when substantial emission starts, the potential of the floating probe commences to rise and at somewhat higher heating current the saturation appears at about -13.5 V, respectively -30 V. Potential of the floating emitting probe in the saturation region is taken as a good

approximation of the plasma potential, therefore a heating current of 2.6 A was chosen for all experiments.

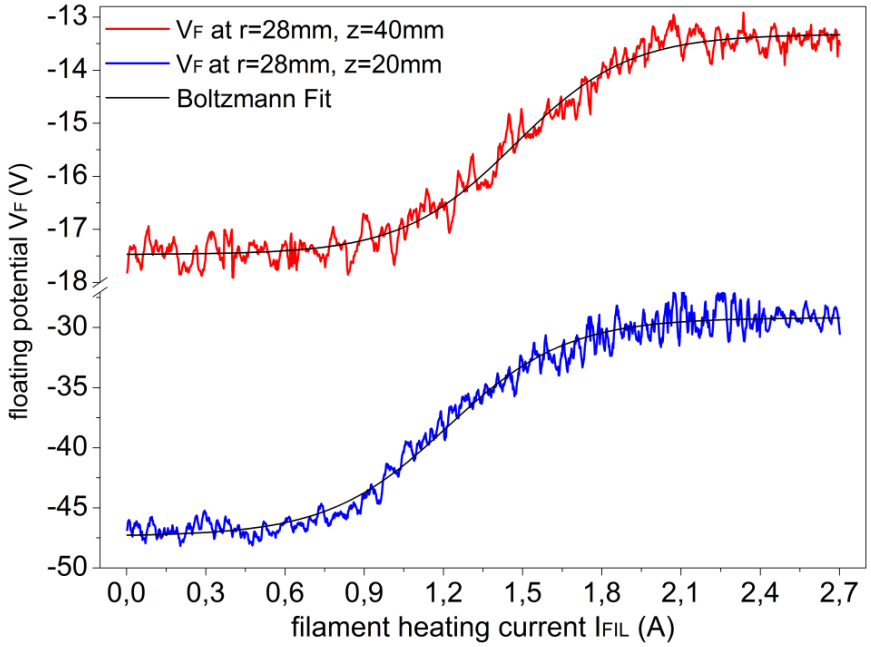

Figure 4 Floating potential as a function of the heating current, at the probe position (r = 28 mm, z = 20mm resp. 40mm). The floating potential approaches to the plasma potential when the heating current exceeds about 2.1 A.

III c. Time-resolved floating and emissive probe measurements:

Time evolution of a typical discharge current $I_D(t)$, plasma potential $V_P(t)$ and floating potential $V_F(t)$ are displayed in Fig. 5. The reference time when the plasma starts, time stamp t=0 s, was defined by the increase of the discharge current in the logarithmic plot as depicted in the inset of the graph. To get rid of the statistical time delay of the discharge onset all measured plasma and floating potential waveforms are referenced to the starting point of the discharge current. All traces are time averaged from 100 discharge pulses, furthermore the standart deviation is plotted. The applied discharge voltage (target voltage relative to the grounded anode) was -488 V and will not be further displayed or discussed because it is constant for the pulses due to the large capacitance of the SPIK2000A pulse power spupply.

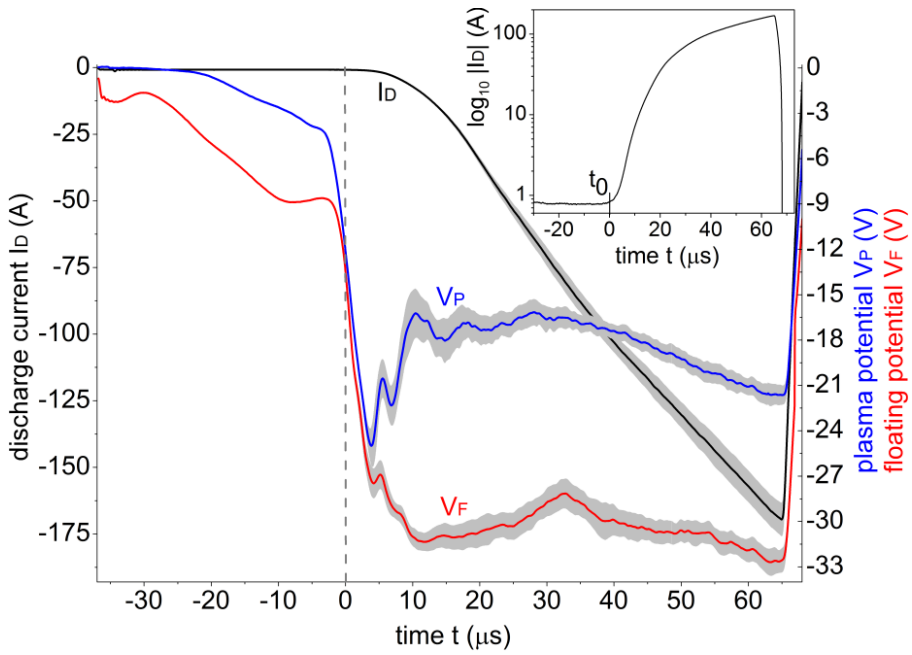

Figure 5 Time evolution of a typical plasma and floating potential waveform measured at position r = 24mm z = 22mm. Additionally the discharge current waveform is shown produced by the SPIK pulser supply for an average power of 240W, pulse width 100us, repetition rate 100Hz and argon gas pressure 0.26 Pa

The discharge current has approximately a triangular shape over the entire pulse period with a maximum current of 170 A since the current has not reached the maximum that could develop for the given voltage.

The electric potential of probes is very sensitive to the balance of charged particles arriving or leaving the probe. The fact that the plasma and floating potential is negative during the initial phase of the pulse shows that weak plasma is already present before the current transformer measure the discharge current.

The plasma potential waveform shows at the initial stage of the discharge an overshoot-like phase; when the plasma potential rapidly drops to negative values, that already happens before the discharge currents I_D measured by the Pearson current transformer indicate negative current values.

After the overshoot phase of V_P the plasma potential rises to a local maximum and then falls subsequently during the pulse on time. The first peak minimum in absolute value is associated with the primary energetic electrons (electron avalanche) generated at the beginning of the discharge, which are repulsed from the target. Gudmundsson et al. showed that the electron density increases initially to a peak value of $3\times10^{18}m^{-3}$ and decrease to $10^{17}m^{-3}$ after several μs, during a 5mTorr Ar-HiPIMS pulse with a tantalum target [17]. The shoulder that follows the first peak in the plasma potential waveform is enhanced by the production of ions and lead up to an increase in the plasma potential[18].

Bohlmark et. al investigated the time depend plasma composition of Ti in Ar. In the first time interval (0–20 μs) mainly Ar ions are recorded, but thereafter highly metallic plasma was measured. During the most intense moment of the discharge, the ion flux consisted of approximately 50% Ti^{1+}, 24% Ti^{2+}, 23% Ar^{1+}, and 3% Ar^{2+} ions[3]. Thus in our experiment, the plasma transforms from Ar-dominated in the beginning of the discharge to Nb ion plasma at a later stage, due to the intensive sputtering of niobium atoms and their more effective ionization(6.76 eV) in the discharge compared to argon(15.76 eV).

IV. RESULTS

IV. a. Time depend plasma potential distribution

The following array of figures shows the time-dependent spatial evolution of the plasma potential distribution measured by the emissive probe and the derived electric field during different times of the HiPIMS pulse.

For best visibility and ease of interpretation, the axes of the plasma potential were adjusted to show the distribution very well.

For a better visualizing of the spatial measured data, a surface was modeled to the data points; using the MATLAB surface fitting algorithm "Gridfit". The electric field distribution $\vec{E} = -\nabla V_P$, has been derived from the surface equations resulting from the gridfit-script.

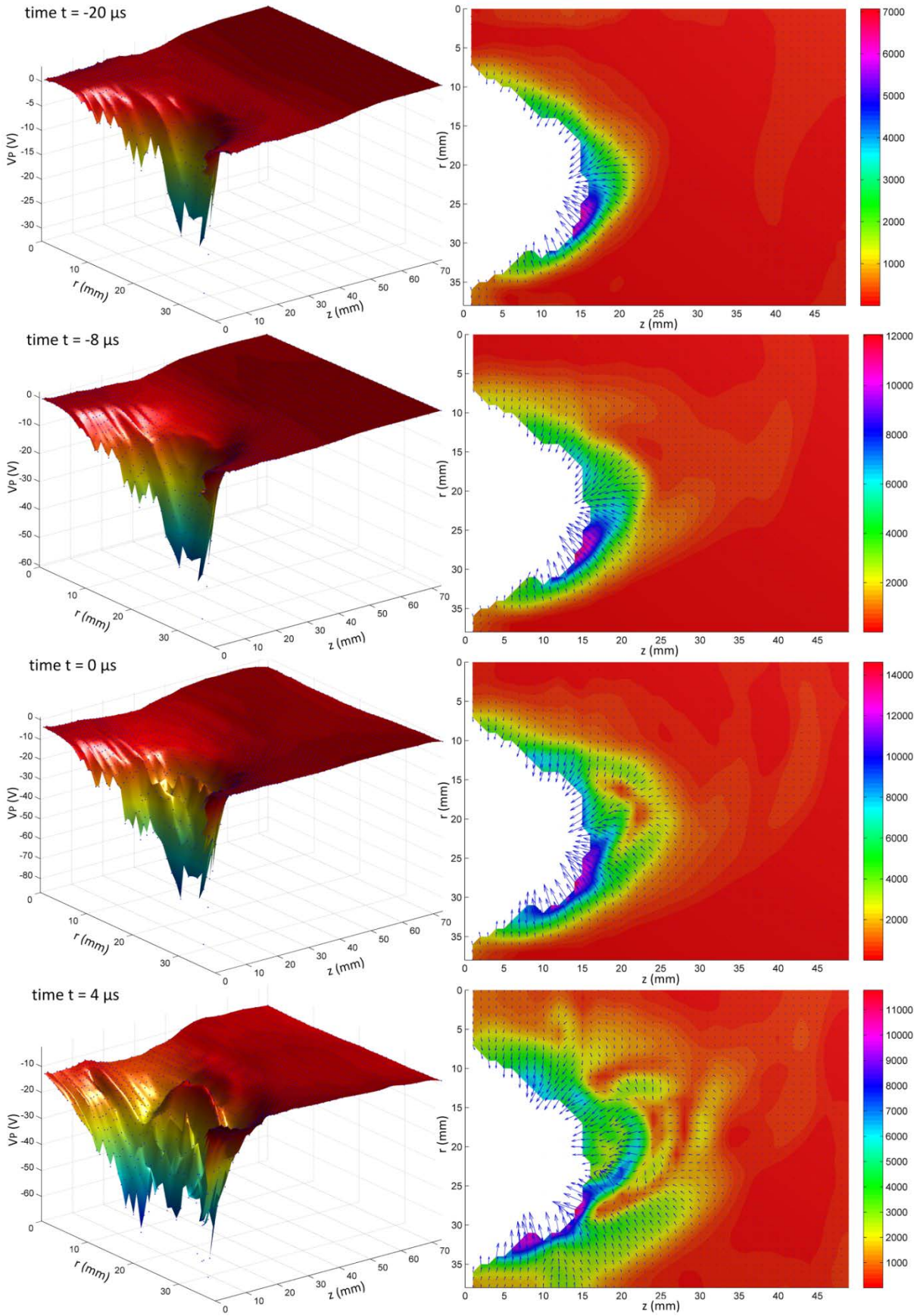
time t = -20 µs
time t = -8 µs
time t = 0 µs
time t = 4 µs
VP (V)
r (mm)
z (mm)

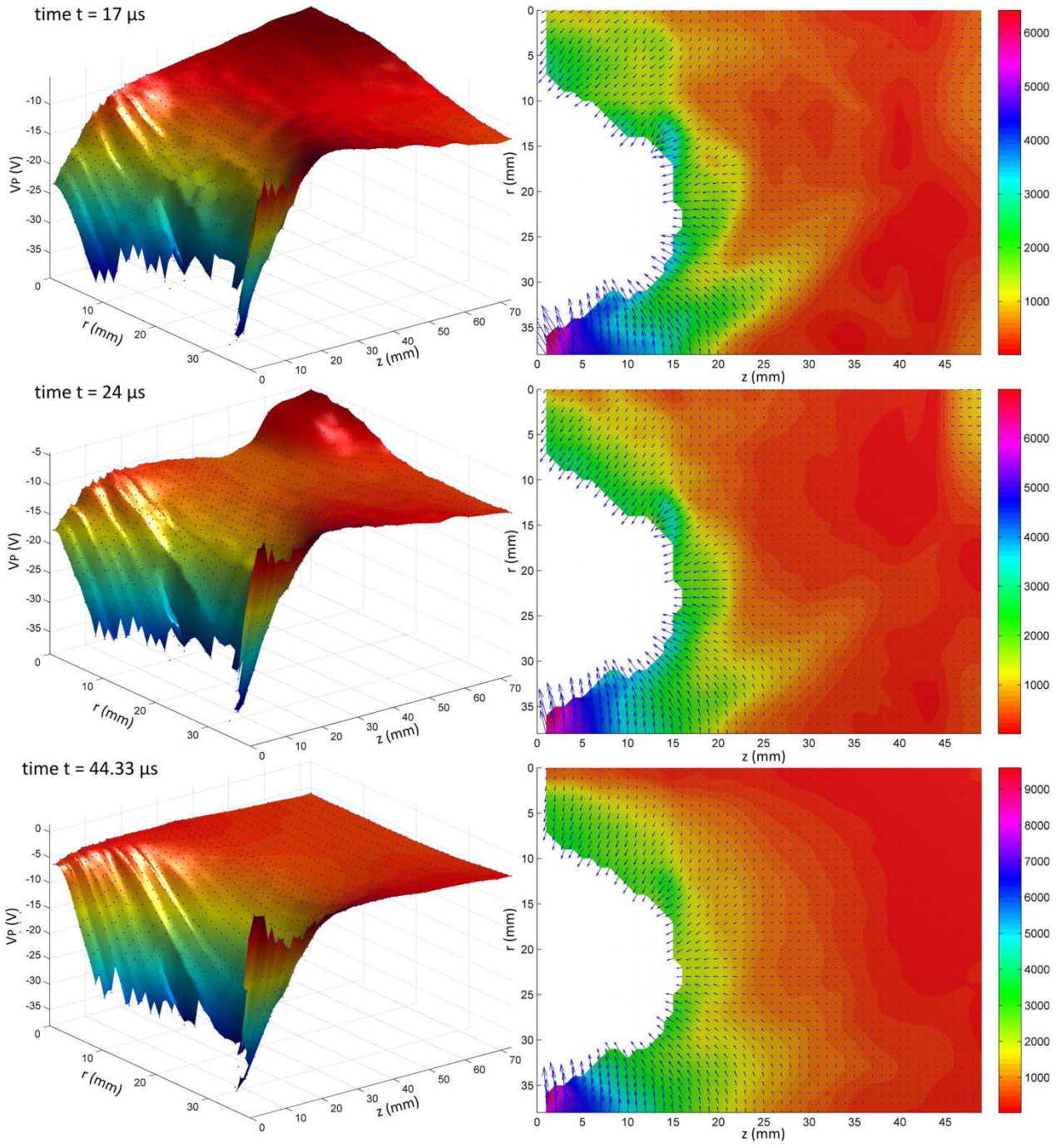

Figure 6 Plasma potential distribution and derived electric field (V/m) for different time stamps during a HiPIMS pulse

The electric field between the cathode (negative) and anode (positive) is highly non-uniform. Once the discharge plasma is established, most of the voltage drop of typically several hundred volts will be located in the space-charge layer, known as the sheath, adjacent to the target surface. The plasma potential becomes more negative with increasing magnetic field due to the better confinement of

the electrons (electron cyclotron radius $r \sim 1/B$). The better confinement is also shown by steeper gradients of the potential and hence strong electric field at the edge of the racetrack region

It attains that there is a maximum potential drop of -90.6 V in the axial direction along the race track line over a distance of 40mm. Therefore plasma potential measurements showed that roughly 20% of the voltage will drop outside the sheath.

The implication is that (a) electrons gain most energy when crossing the sheath coming from the target surface (i.e. the secondary electrons are the most energetic), and (b) plasma electrons, which have typically only a few eV of energy, cannot penetrate the sheath but "bounce off" and return to the plasma. Ions are generally not magnetized in sputtering magnetrons since their gyration radius usually exceed the characteristic system length. Ions are accelerated by the electric field, positive ions towards the target, and negative away. Sputtering of surface atoms from the target is really based on the last "kick" that positive ions obtain in the sheath before impacting the target surface.

During the overshoot when the cathode sheath expands (ignition phase t = 0s) the plasma potential distribution is highly unstable when the discharge current increases after a time span of about *10 μs* it relaxes to a more homogeneous distribution even though the discharge current increases more and more until the pulse stops. Electrons have a very high mobility so the redistribution happens very fast in a nanosecond timescale, according to the plasma frequency $f_{pe} = 8980 * \sqrt{n_e}$, where n_e is the electron density.

In the outer regions *z ϵ (40,72)mm* the magnetic field lines are not closed anymore, there the plasma potential reveals much smaller spatial and temporal variations in the range of -10 to 0V with very less electric fields.

The electric field is not everywhere directed towards the target; in regions z < 45mm (*time t=4 μs*) an electric field reversal can be found where a considerable electric field pointing away from the target. This region also called extended presheath. Brenning et.al. identified the high value of the transverse resistivity $\eta_\perp$ having a fundamental importance both for the potentials profiles and for the motion of ionized target material through the bulk plasma, and that the electric field reversal is a consequence of the high value of $\eta_\perp$[19]. This reversal of the electric field means that ions with low energies will be accelerated outwards or be trapped, and not be drawn back to the target. The rising potential also acts as a barrier to the ions reaching the substrate. The potential wave which is visible in the pictures (time t= 4us and time t= 24us) propagates with about 1800m/s away from the target off wards from the target.

Bohlmark et al. showed that a high-density doughnut shaped plasma forms above the race track in the early stage of a HiPIMS discharge. The high density plasma expands in the later stage of the discharge away from the target surface in the z direction, but also in the radial direction[20].

Due to the much higher mass of the ions in the plasma (Ar^+ ion to electron mass ratio M_i/m_e is 1835/40), their Larmor radii are greater than the dimension of the plasma. Therefore, they are assumed to be non-magnetized, consequently the arrows of the electric field indicate the ion trajectories based on the electric force $\vec{F} = q \cdot \vec{E}$.

IV. c. Electron velocity distribution for the ExB-direction:

Combining the derived electric field $\vec{E}$ and the measured magnetic field $\vec{B}$ the distribution of a single particle $\vec{E}$ x $\vec{B}$ drift can be found. From the plot of the magnetic field lines $\vec{B}$ and the derived electric field $\vec{E}$ it can be seen that there is a region above the target, where these two vector fields are perpendicular to each other. Therefore magnetized electrons experience an azimuthal $\vec{E}$ x $\vec{B}$ drift, this constitutes a confined closed-loop Hall current flowing in a channel above the racetrack, which may be many times larger than the discharge current I_D.

The trajectories of the ions are mostly insensitive to the magnetic field due to their much higher Larmor radii, therefore, they are assumed to be non-magnetized and do not experience these drifts.

If a component in $\vec{E}$ x $\vec{B}$ exists, the magnetized electrons will drift in that direction with a drift velocity $\overrightarrow{v_D}$ of their guiding center

$$\overrightarrow{v_D} = \frac{\vec{E} \times \vec{B}}{B^2} \qquad 4)$$

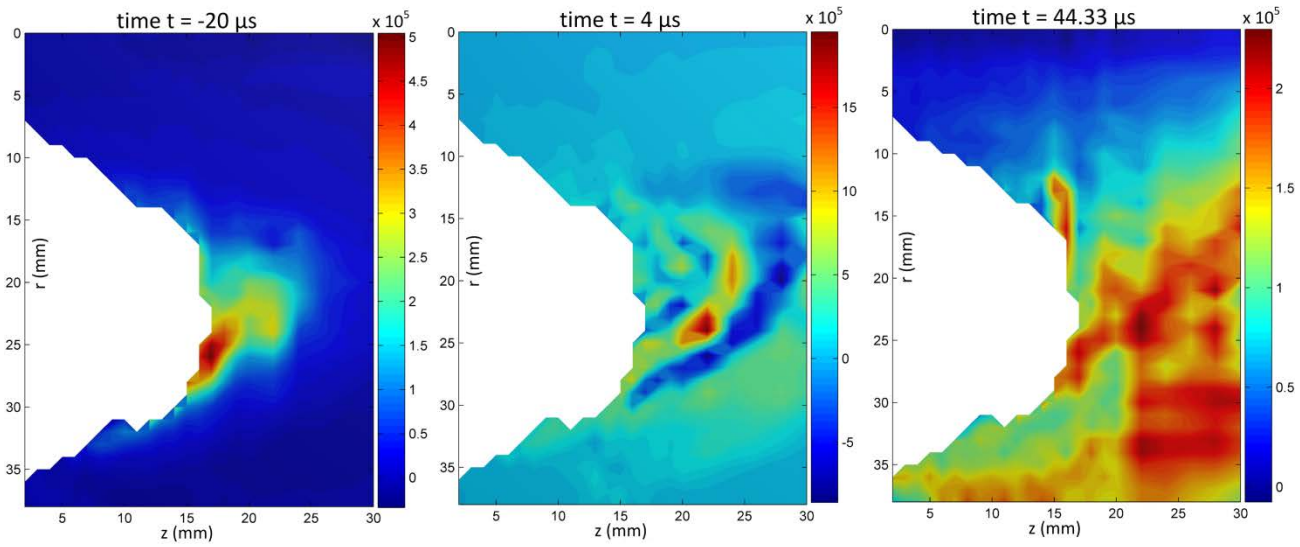

Figure 7 Distribution of ExB velocities

From the E and B field distribution the azimuthal $\vec{E}$ x $\vec{B}$ drift velocity was calculated using equation 2) and is shown in Fig 10 for three different timestamps, at the beginning, middle and end of the HiPIMS pulse. Positive values in the contour plot are going into the r-z plain.

Mostly in all parts of the discharge the Hall drift acts in the same direction with a value in the range 10^5 ms^{-1}. When the discharge current kicks in, islands are formed with opposite drift directions, depending on the orientation of the electric field. Assuming an electron temperature of 2 eV, which is approximately the temperature of the lower energy electrons in the non-Maxwellian plasma, corresponds to electron Larmor radii for z>30mm in the range of cm (>1.5cm). Therefore we assume that the electrons in the z>30mm region are not magnetized and do not or less contribute to the Hall drift.

ACKNOWLEDGMENTS

We gratefully acknowledge help by Dr. S. Lim and J. Wallig for assistance in probe construction and vacuum technology. A. Rauch thanks the Austrian Marshall Plan Foundation (www.marshallplan.at) for funding a scholarship.

J.M. Sanders thanks the AFOSR for supporting his Ph.D. research. This work was done at Lawrence Berkeley National Laboratory with support by U.S. Department of Energy under

V REFERENCE

1. Helmersson, U., Lattemann, M., Bohlmark, J., Ehiasarian, A.P. & Gudmundsson, J.T. Ionized physical vapor deposition (IPVD): A review of technology and applications. *Thin Solid Films* 513, 1-24 (2006).

2. André, A. Discharge physics of high power impulse magnetron sputtering. *Surface and Coatings Technology* 205, Supplement 2, S1-S9 (2011).

3. Bohlmark, J. et al. The ion energy distributions and ion flux composition from a high power impulse magnetron sputtering discharge. *Thin Solid Films* 515, 1522-1526 (2006).

4. Ehiasarian, A.P. et al. Influence of high power densities on the composition of pulsed magnetron plasmas. *Vacuum* 65, 147-154 (2002).

5. Rossnagel, S.M. & Kaufman, H.R. Induced drift currents in circular planar magnetrons, Vol. 5. (AVS, 1987).

6. Lundin, D. & et al. Anomalous electron transport in high power impulse magnetron sputtering. *Plasma Sources Science and Technology* 17, 025007 (2008).

7. Hecimovic, A. & Ehiasarian, A.P. Time evolution of ion energies in HIPIMS of chromium plasma discharge. *Journal of Physics D: Applied Physics* 42, 135209 (2009).

8. Vetushka, A., Karkari, S.K. & Bradley, J.W. Two-dimensional spatial survey of the plasma potential and electric field in a pulsed bipolar magnetron discharge, Vol. 22. (AVS, 2004).

9. Poolcharuansin, P. & Bradley, J.W. Short- and long-term plasma phenomena in a HiPIMS discharge. *Plasma Sources Science and Technology* 19, 025010 (2010).

10. Bradley, J.W. & et al. Measurement of the plasma potential in a magnetron discharge and the prediction of the electron drift speeds. *Plasma Sources Science and Technology* 10, 490 (2001).

11. Mravlag, E. & Krumm, P. Space potential measurements with a continuously emitting probe, Vol. 61. (AIP, 1990).

12. Balan, P. et al. Emissive probe measurements of plasma potential fluctuations in the edge plasma regions of tokamaks, Vol. 74. (AIP, 2003).

13. Hershkowitz, N. How does the potential get from A to B in a plasma? . *Plasma Science, IEEE Transactions on* 22, 11-21 (1994).

14. Bradley, J.W. & et al. Measurements of the sheath potential in low density plasmas. *Journal of Physics D: Applied Physics* 25, 1443 (1992).

15. Sanders, J.M., Rauch, A., Mendelsberg, R.J. & Anders, A. A synchronized emissive probe for time-resolved plasma potential measurements of pulsed discharges. *Review of Scientific Instruments* 82, 093505-093507 (2011).

16. Gudmundsson, J.T., Alami, J. & Helmersson, U. Evolution of the electron energy distribution and plasma parameters in a pulsed magnetron discharge, Vol. 78. (AIP, 2001).

17. Gudmundsson, J.T. The high power impulse magnetron sputtering discharge as an ionized physical vapor deposition tool. *Vacuum* 84, 1360-1364 (2010).

18. Jouan, P.Y. et al. HiPIMS Ion Energy Distribution Measurements in Reactive Mode. *Plasma Science, IEEE Transactions on* 38, 3089-3094 (2010).

19. Brenning, N., Axnäs, I., Raadu, M.A., Lundin, D. & Helmerson, U. A bulk plasma model for dc and HiPIMS magnetrons. *Plasma Sources Science and Technology* 17, 045009 (2008).

20. Bohlmark, J.G., J.T.; Alami, J.; Latteman, M.; Helmersson, U.; Spatial electron density distribution in a high-power pulsed magnetron discharge *Dept. of Phys. & Meas. Technol.* 33, 346-347 (2005).